UCRL-ID-142949

New Front End Technology

D. Pennington, I. Jovanovic, B. J. Comaskey

February 1, 2001

U.S. Department of Energy

Lawrence
Livermore
National
Laboratory

DISCLAIMER

This work was performed under the auspices of the U. S. Department of Energy by the University of California, Lawrence Livermore National Laboratory under Contract No. W-7405-Eng-48.

New Front End Technology

D. Pennington, I. Jovanovic, B. J. Comaskey

00-ERD-070

FY00 LDRD Annual Report

February 2001

Lawrence Livermore National Laboratory, Livermore, California 94550

Abstract

The next generation of Petawatt class lasers will require the development of new laser technology. Optical parametric chirped pulse amplification (OPCPA) holds a potential to increase the peak power level to >10 PW with existing grating technology through ultrashort pulses. Furthermore, by utilizing a new type of front-end system based on optical parametric amplification, pulses can be produced with substantially higher contrast than with Ti:sapphire regenerative amplifier technology. We performed extensive study of OPCPA using a single crystal-based OPA. We developed a replacement for Ti:sapphire regenerative amplifier for high peak power lasers based on OPCPA, with an output of 30 mJ at 10 Hz repetition rate and 16.5 nm spectral bandwidth. We developed a 3D numerical model for OPCPA and we performed a theoretical study of influences of pump laser beam quality on optical parametric amplification. Our results indicate that OPCPA represents a valid replacement for Ti:sapphire in the front end of high energy short pulse lasers.

Contents

1. Introduction

Current high peak power laser systems based on chirped pulse amplification are built on a hybrid technology. Ti:sapphire regenerative amplifiers are used as preamplifiers, due to their intrinsic large gain bandwidth. Chirped pulses amplified to ~50 mJ level are subsequently injected into high energy storage media such as Nd:glass, where they can be amplified to high energy levels. Pulses experience gain narrowing in Nd:glass amplifiers, which generally limits the pulse duration to several hundreds of femtoseconds. The advantage of using the broadband gain media as preamplifiers is in reduced level of gain narrowing compared to systems based on Nd:glass only, which increases the attainable peak power from the system.

One problem that poses severe difficulties in usage of Ti:sapphire-Nd:glass systems is the level of prepulse. In target experiments where focused intensities of up to 10^{21} W/cm^2 are involved, a 10^{-2} - 10^{-3} level of prepulse can significantly perturb the target before the arrival of the main pulse. The contributing factors to pulse contrast include amplified spontaneous emission (ASE), leakage from regenerative amplifiers and hard-edge spectral clipping on the compressor gratings. During the regenerative (multipass) amplification process, each time the pulse completes one round-trip in the multipass cavity, a small fraction (~1%) leaks out of the cavity. Hence, the system produces prepulses spaced one cavity round-trip time ahead of the main pulse. While spectral clipping can be eliminated by using larger compressor gratings, the pulse contrast remains fundamentally limited by the ASE and leakage from regenerative amplifiers.

Here, we describe the development of new front-end technology for all chirped-pulse amplified systems which does not utilize regenerative amplifiers or Ti:sapphire. Used extensively for laser frequency multiplication and generation of tunable radiation, nonlinear optical materials configured as optical parametric amplifiers (OPAs) can be used as gain media. The fundamental difference between the conventional laser amplifiers and OPAs is the amplification mechanism, which in OPAs utilizes instantaneous nonlinear wave interaction rather than energy storage and stimulated emission. Optical parametric amplification is a three-wave mixing process in which pump, signal and idler waves are involved. A low intensity signal wave (seed) is incident

on a nonlinear medium together with a high intensity pump wave. Through the difference frequency generation process, an idler wave is generated at the difference frequency between the pump and the signal wave. Simultaneously, the intensity of the signal wave is increased. Since there is no gain of the signal without the presence of the pump wave, pumping the nonlinear crystal with a short (~1 ns) pump pulse eliminates any possiblitity of amplified sponaneous emission coming earlier than the pump pulse. Furthermore, since single pass gains as high as 10^4 can be achieved in this process, there is no need for regenerative (multipass) amplification.

Our current experience with nonlinear materials leads us to selection of novel materials such as -barium borate (BBO), due to large effective nonlinearity, high damage threshold and broad bandwidth, whenever such selection is possible. The calculated angular tolerance is 0.4 mrad for a 15 mm BBO crystal, which implies that we need a good beam quality to ensure that the majority of the wavevectors have orientations which fall within the angular tolerance limit. We calculate spectral bandwidth of 53 nm for a 15 mm BBO crystal and 80 nm for a 10 mm BBO crystal. These values can be experimentally confirmed by measuring the parametric fluorescence bandwidth of the optical parametric generator (OPG).

With current chirped pulse amplification laser systems, laser peak power is limited by the energy handling limits of the compressor gratings. The route to increase laser power further then lies with utilization of shorter pulses and large bandwidth amplifiers such as optical parametric amplifiers. A theoretical study has shown that without advances in the grating technology, optical parametric chirped pulse amplifiers could be constructed with peak powers up to 15 PW. Focused intensities would approach 10^{23} W cm^{-2} and open a new class of physical phenomena accessible to laser experimenters.

We describe the activities and outcome of our study by first descibing a numerical model that we developed to predict the performance of OPA in nanosecond pulse regime, followed by the experiments using single OPA crystal. We designed and built an OPCPA system based on a commerical pump laser and we characterized its output. Additionally, we addressed the problem of the impact of pump laser beam quality on amplification and conversion efficiency in optical parametric amplification.

2. Development of a 3D numerical model

Our model is based on a numerical solution of the system of coupled differential equations for difference frequency generation. The system can be written in a concise form as

$$\frac{dA_s}{dz} = i\frac{2\omega_s}{n_s c} d_{eff} A_p A_i^* \exp(i\Delta kz),$$

$$\frac{dA_i}{dz} = i\frac{2\omega_i}{n_i c} d_{eff} A_p A_s^* \exp(i\Delta kz), \qquad (1)$$

$$\frac{dA_p}{dz} = i\frac{2\omega_p}{n_p c} d_{eff} A_i A_s \exp(-i\Delta kz),$$

where by A_s, A_i and A_p we denote the amplitude of the electric field of the signal, idler and pump, respectively, d_{eff} is effective nonlinearity. Since our interest in OPCPA is focused on pulses which are relatively long (nanoseconds), effects of temporal walk-off due to group velocity dispersion can be neglected. Additionally, our model is simplified to disregard diffraction effects, which is a valid approximation when relatively weak beam focusing is involved, such as in nanosecond OPA.

Eqs. (1) model the interaction of plane waves and have to be suitably modified to describe the situation where the beam diameter is finite and the beam has a specific transverse intensity profile. In addition, temporal modulation of the pulse will occur due to variable intensity during the temporal evolution of the laser pulse. Finally, the effect of Poynting vector walk-off for extraordinary waves in birefringent crystals presents an additional effect that requires inclusion in the model, particularly when beam diameter is comparable to total walk-off over the crystal length.

We proceed to evaluate those effects by solving the Eqs. (1) for traveling waves numerically on a 3-dimensional grid in space and time. We start with the assumed intensity distribution of the original waves at a point:

$$I_\alpha(x,y,t) = 2n_\alpha \frac{\varepsilon_0}{\mu_0} \left| A_\alpha(x,y,t) \right|^2, \qquad (2)$$

where x and y denote two transverse dimensions, and t denotes the temporal dimension. The intensity distribution is normalized in the following fashion:

$$\int_{-\infty}^{\infty}\int_{-\infty}^{\infty}\int_{-\infty}^{\infty} I_\alpha(x,y,t)dxdydt = E_\alpha \,, \tag{3}$$

where E_α is the total pulse energy. We assign a zero phase to the electric field of the seed and pump at the input face of the crystal (z=0), consistent with invariance of optical parametric amplification on the initial phase relationship between the seed and the pump, prior to the idler build-up. Additionally, we introduce the effect of pump beam walk-off angle ρ in one direction (x) and noncollinear angle in two directions for signal (Ω_{sx}, Ω_{sy}) and idler beam (Ω_{ix}, Ω_{iy}), and by correcting for the appropriate component of the pump, signal and idler beam at the specific point z in the crystal:

$$x_p^{corr} = x_p + \rho\, z\,, \tag{4}$$

$$x_s^{corr} = x_s + \Omega_{sx} z\,,\ y_s^{corr} = y_s + \Omega_{sy} z\,, \tag{5}$$

$$x_i^{corr} = x_i + \Omega_{ix} z\,,\ y_i^{corr} = y_i + \Omega_{iy} z\,. \tag{6}$$

In chirped pulse amplification the spectrum is linearly chirped in time, so the phase mismatch due to spectral bandwidth can be included by assigning the appropriate value for wavevector mismatch for each point in time and its projection in the direction normal to the crystal surface:

$$\mathbf{\Delta k}(t) = \mathbf{k}_\mathrm{p} - \mathbf{k}_\mathrm{s}(t) - \mathbf{k}_\mathrm{i}(t), \tag{7}$$

$$\Delta k_z(t) \approx 2\pi\left(\frac{n_p}{\lambda_p} - \frac{n_s(t)}{\lambda_p(t)} - \frac{n_i(t)}{\lambda_i(t)}\right) \tag{8}$$

Finally, the system of differential equations can be now written at the point in time t as

$$\begin{aligned}
\frac{dA_s(x_s^{corr}, y_s^{corr}, t)}{dz} &= i\frac{2\omega_s(t)}{n_s(t)c} d_{eff} A_p(x_p^{corr}, y, t) A_i^*(x_i^{corr}, y_i^{corr}, t)\exp(i\Delta k(t) z),\\
\frac{dA_i(x_i^{corr}, y_i^{corr}, t)}{dz} &= i\frac{2\omega_i(t)}{n_i(t)c} d_{eff} A_p(x_p^{corr}, y, t) A_s^*(x_s^{corr}, y_s^{corr}, t)\exp(i\Delta k(t) z),\\
\frac{dA_p(x_p^{corr}, y, t)}{dz} &= i\frac{2\omega_p(t)}{n_p(t)c} d_{eff} A_i(x_i^{corr}, y_i^{corr}, t) A_s(x_s^{corr}, y_s^{corr}, t)\exp(-i\Delta k(t) z).
\end{aligned} \tag{9}$$

We now calculate the electric field on the grid of (*DX*, *DY*, *DT*) points with a spatial and temporal window size (*WX*, *WY*, *WT*), such that the following normalization condition applies:

$$2n_\alpha \frac{\varepsilon_0}{\mu_0} \frac{WX}{DX} \frac{WY}{DY} \frac{WT}{DT} \sum_{j=1}^{DX} \sum_{k=1}^{DY} \sum_{l=1}^{DT} \left| A_\alpha(j,k,l) \right|^2 = E_\alpha \,. \tag{10}$$

The system (9) in discrete form is solved numerically using a 4th order Runge-Kutta integration routine, yielding solutions for electric field amplitude and phase at the crystal output, in a spatially and temporally resolved form. It is important to note that the model allows initial misalignment of the seed and pump beam at the nonlinear crystal, which is a frequent experimental optimization procedure required to achieve best overlap of the beams inside a crystal which exhibits walk-off properties for one of the beams.

No explicit modeling has been included for the diffraction effects in the model due to their weak relative impact compared with the temporal and spatial modulation. In particular, two effects due to diffraction can be identified that can influence gain and conversion efficiency in optical parametric amplification. First, variable beam diameter causes nonuniform intensity along the crystal. Second, diffracted angle leads to dephasing between the beams and reduced gain due to finite angular acceptance of the nonlinear crystals. Both of these effects are weak with weakly focused beams, which are used in nanosecond OPCPA, and do not play an important role in the amplification process.

3. Single crystal OPCPA experiments

Several previous studies demonstrated high gain and bandwidth in OPCPA; most notably, up to 0.5 J of power has been generated in OPCPA system and the pulses were successfully recompressed. Pump to signal conversion efficiency achieved was 25% in periodically poled materials. However, no particular attention has been given to rigorous prediction of gain and conversion efficiency in OPCPA when real laser beams with various spatial and temporal beam profiles are used. In particular, the use of standard Q-switched Nd:YAG lasers widely used for pumping Ti:sapphire to pump OPAs is of great practical interest, with possible OPA potential to entirely replace Ti:sapphire. It is therefore important to evaluate the utility of standard Q-switched lasers for pumping optical parametric chirped pulse amplifiers. In this part of our study we focused on the prospects and limitations in OPCPA imposed by the use of pump lasers with unstable resonators.

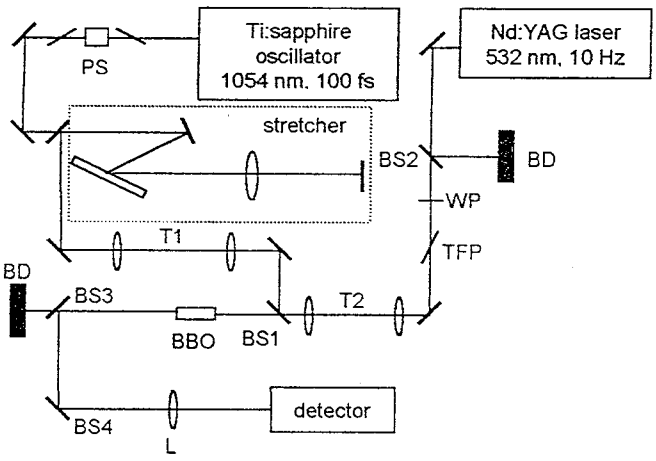

Figure 1.

Our experimental system (Fig. 1) starts with a commercial mode locked Ti:sapphire oscillator, with a central wavelength of 1059 nm and 16.5 nm bandwidth, producing tranform-limited 100 fs pulses. A pulse selector PS is introduced after the oscillator, selecting individual pulses from the oscillator pulse train at 10 Hz repetition rate. The pulses are subsequently introduced into the stretcher, consisting of a single

grating and lens, with a stretching ratio of $>2x10^4$. The output is in the form of 2.65 ns pulses, with spectrum clipped at 15 nm FWHM (Fig. 2). The seed beam is collimated and imaged using telescope T1, and introduced into the crystal by reflection from a dichroic beamsplitter BS1. The pump beam is provided by a commercial Nd:YAG frequency-doubled laser, producing >600 mJ of 532 nm pulses at 10 Hz repetition rate, and with pulse width ~8.5 ns. The pump laser is based on an unstable resonator configuration, and was upgraded for injection seeding. Single longitudinal mode operation is crucial in OPCPA, which requires stable temporal pulse waveform to avoid extensive spectral modulation and crystal damage from high intensity spikes produced in unseeded laser resonator.

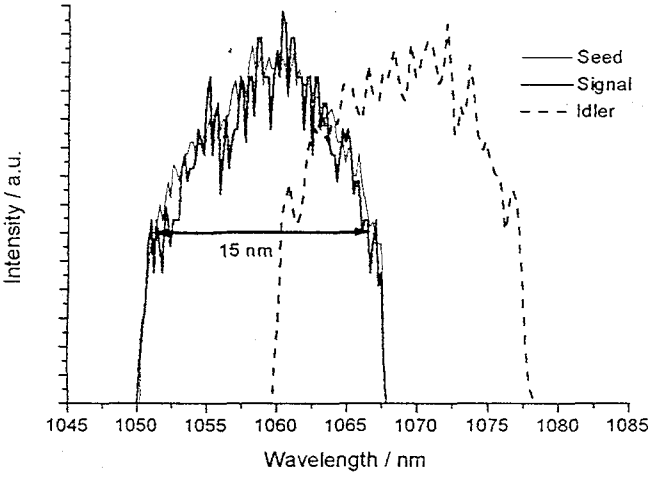

Figure 2.

Beamsplitter BS2 transmits 20% of the pump beam, and a waveplate-polarizer combination (WP-TFP) is introduced in order to vary the pump energy in a controllable fashion. The beam is resized, collimated and imaged onto the crystal using telescope T2. We used two crystals in our investigation: the first is a 4x4x15 mm BBO crystal, and the second is a 4x4x10 mm BBO crystal. The first crytal was uncoated, while the second crystal was AR coated for 1064/532 nm. Both crystals had a 2° wedge on one crystal face, preventing parasitic oscillation from developing when signal or idler reflect from the crystal back surface. Crystals were cut at φ=0° and θ=22.8°, phase matching angle for a type I difference frequency mixing process 1059 nm (o) + 1069 nm (o) = 532 nm (e).

Amplified pulses are separated from the pump beam using two dichroic beamsplitters (BS3 and BS4), and the noncollinear idler beam is separated from the signal using a knife-edge beam separator. The amplified signal beam is focused entirely onto a fast silicon diode detector, which is used for diagnostics. The idler beam is also imaged onto a CCD camera to examine the near field spatial beam profile.

We first measured spatially resolved temporal evolution of the pump pulse. For this purpose, the pump laser beam at the OPA crystal was suitably magnified and relay imaged onto a 400 μm pinhole, and a fast silicon diode detector was centered behind the pinhole. Amplitude, pulsewidth and build-up delay were recorded as a function of radial position of the pinhole and the results are shown in Fig. 3.

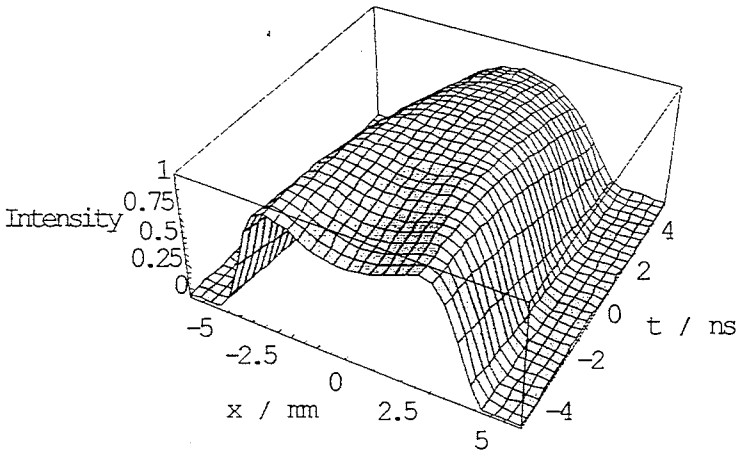

Figure 3.

A significant build-up delay and difference in pulsewidth exists for different radial positions in the pump beam, as a result of pulse build-up in an unstable resonator in the pump laser. While the center of the pump pulse has a slowly variable build-up delay as a function of radial position when compared to the position in the wings of the pump beam, its pulsewidth is longest at the beam center. This is a particular difficulty for use in optical parametric amplification, which requires high beam intensities a shorter pulses. Additionally, we anticipate the problem of Poynting vector walk-off to be more critical in OPA pumped by this pulse compared to a pulse which has no radial distribution of build-up delay. This is the result of the instantaneous effective beam size in interaction smaller

than the temporally integrated beam size, giving rise to reduced overlap between the signal and the pump beam.

Another consideration in OPA pumped by a pump laser with pulsewidth longer than the seed pulsewidth is the possibility of high extraction efficiency. While it is possible to extract more energy from a long pump pulse by consecutive amplification in multiple OPAs using variable seed delay (temporal multiplexing), this extraction becomes more difficult when the pump pulse exhibits spatio-temporal evolution determined by the unstable resonator, where the back of the pulse acquires a "donut" shape. In this case only a narrow range of temporal slices of the pump pulses is usable for OPA. Our experiment was performed with seed beam diameter comparable to the pump beam diameter. Fig. 4 shows the recorded seed and pump beam profiles. Seed exhibited gaussian beam profile, with $1/e^2$ diameter of 0.4 mm, and the pump beam had near 8th order supergaussian beam profile, with $1/e^2$ diameter of 1.6 mm. The incident pump pulse energy was up to 88 mJ, while the seed pulse energy was 500 pJ. Seed was injected noncollinearly into the crystal, at 0.5° angle with respect to the pump beam, perpendicular to the crystal principal plane. A displacement was introduced between the center of the seed and the center of the pump beam at the entrance face of the crystal to improve the spatial overlap in the crystal, which is reduced by pump beam walk-off. The calculated displacement that maximizes gain in the small signal regime is the half of the walk-off distance, which is 0.56 mm per 1 cm of crystal length in BBO. Figs. 4-5 show the gain measured for a 10 mm and 15 mm crystal, together with an theoretical calculation based on finite element method of calculation on the spatio-temporal mesh, as described in the previous section. Excellent agreement is evident between the experimental and the theoretical results.

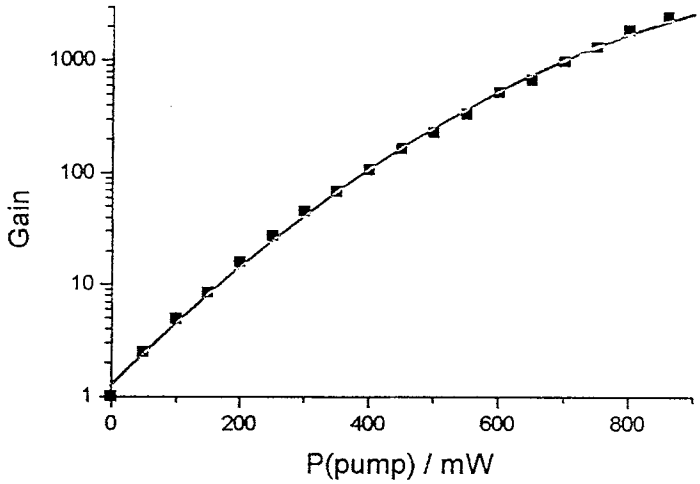

Figure 4.

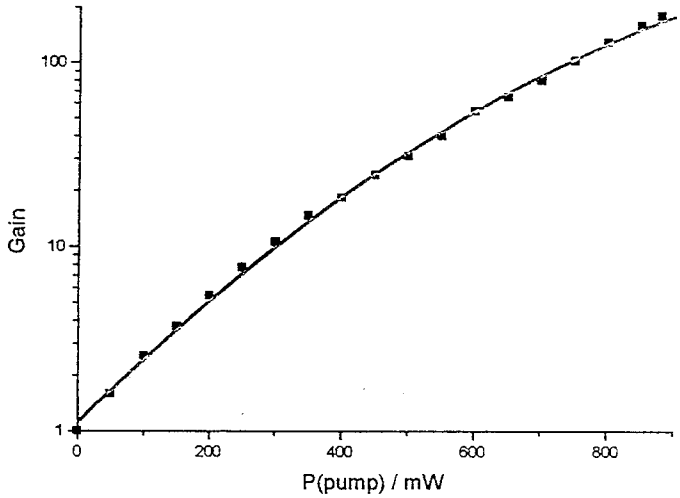

Figure 5.

Although our experiments were performed in the regime where pump depletion is negligible, we expect that the unstable resonator pulse evolution will represent a significant obstacle towards obtaining large conversion efficiency in OPCPA. While ideal pump pulse in OPCPA constitutes a top-hat profile in space and in time, we expect that even elimination of variable build-up delay across the pulse should have a significant positive impact on gain and conversion efficiency, when beam overlap in space and in time is improved.

4. High energy OPCPA experiments

Since the first successful demonstration of OPCPA, experiments were performed which produced up to 0.5 J of amplified pulse with pulse recompression down to 300 fs. Commercial Q-switched pump lasers were used to amplify oscillator pulses up to 600 μJ, and broad amplified bandwidth was observed in all experiments. However, pump-to-signal conversion efficiency from simple, long pulse (~10 ns) pump lasers has not exceeded 0.6 %, limiting the potential attractiveness of OPCPA to facilities with high energy, shorter pulse pump lasers. An exception is OPCPA performed in PPLN, where conversion efficiency up to 20% has been achieved, but no high energy scaling is foreseeable due to crystal aperture limitations.

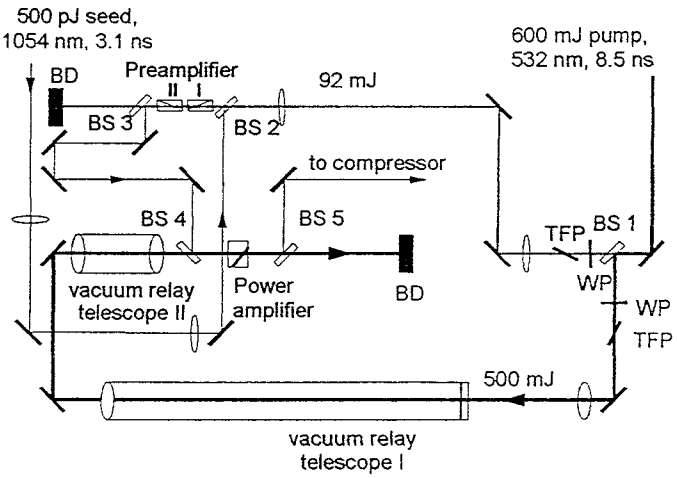

Figure 6.

The design of our system is presented in Fig. 6. A mode-locked Ti:sapphire oscillator with a center wavelength of 1054 nm provides 100 fs transform limited pulses. A single pulse is selected from the oscillator pulse train and stretched using a diffractive grating stretcher configured to clip the spectrum with the bandwidth of 16.5 nm. The stretched pulse width is 3 ns, and the stretched pulse energy is 500 pJ. Our pump laser is a commercial, injection seeded single longitudinal mode Nd:YAG laser, producing 600 mJ of 532 nm output in 8.5 ns pulses at 10 Hz repetition rate. The transverse intensity profile of the pump beam is a supergaussian, while the temporal profile is gaussian, with

a characteristic pulse spatio-temporal evolution for an unstable resonator. The optical parametric amplifier consist of three β-barium borate (BBO) crystals. The size of the first two crystals is 4x4x15mm, and one of them is AR coated for 532 nm and 1064 nm, while the other one is uncoated. The size of the third crystal is 10x10x10 mm, permitting scaling to large incident pump pulse energy by increasing the pump beam diameter. The crystals are cut at 22.8 to allow type I angular phase matching, and they have a 2° wedge on their output faces to prevent intra-crystal parasitic oscillation. The first two crystals are configured as preamplifiers and separated by 2 mm. Walk-off compensation scheme is used in order to decrease the effect of the intrinsic 3.2 extraordinary beam Poynting vector walk-off in BBO. The pump beam is split by a 15% beamsplitter into a 90 mJ beam and a 510 mJ beam. Supergaussian transverse intensity profile of the pump laser is relay imaged between the first two BBO crystals by means of telescope T1, which also adjusts the pump beam size in the first two crystals to 1.6 mm. The peak intensity of the pump beam in the first and second BBO crystal is 450 MW/cm^2 and 430 MW/cm^2, respectively. The pump beam is collimated in order to minimize dephasing due to small angular acceptance of BBO (0.4 mrad cm). An additional source of dephasing is the imperfect beam quality from the pump laser (we measured M^2=1.6 in BBO principal plane). We calculate that the measured imperfect beam quality has negligible impact on parametric gain with the selected beam diameter. The size of the seed beam is dictated by the requirement to avoid spatial modulation on the signal beam due to non-uniform spatial intensity profile of the pump beam and walk-off, and is set to 0.7 mm in the first two BBO crystals. We treat our first two crystals as large-gain preamplifiers and neglect the low conversion efficiency which results from small spatio-temporal overlap of the seed and the pump pulses. The seed beam is introduced into the crystal at 1° angle with respect to the pump beam, perpendicular to the crystal principal plane. The output from the first BBO crystal was 1.8 μJ, (G=3700), and from the second BBO crystal we obtained 1.5 mJ (G=830). Signal pulsewidth after passing through the preamplifier was 3 ns, identical to the original stretched pulse duration as a result of negligible temporal modulation introduced by the pump. The amplified signal and the idler beam are separated spatially after propagating 30 cm out of the preamplifier.

We use the beam transmitted through the 20% beamsplitter BS1 (510 mJ) and

relay image the supergaussian spatial profile of the pump beam onto our final BBO crystal (power amplifier). The imaging telescope contains two vacuum tubes introduced to prevent the ionization breakdown in the air. Pump beam diameter is reduced to 3.5 mm, with peak intensity of 400 MW/cm^2 on the crystal and the expected small signal gain of 75. We measure a saturated gain of 20 from the power amplifier, which amplifies the signal beam up to 30 mJ level with 1.5 mJ produced in the preamplifier.

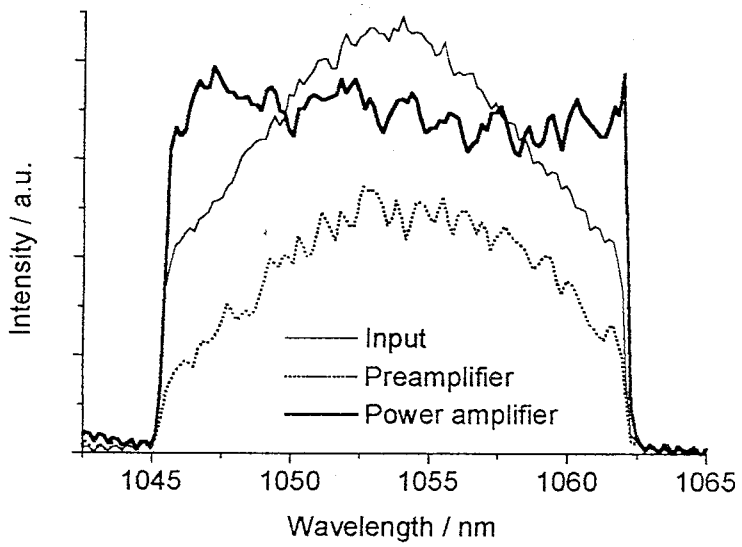

Figure 7.

Signal and idler are separated after 2 meters of propagation out of the power amplifier crystal. We measured the bandwidth of our output beam to be 16.5 nm, which is consistent with the absence of bandwidth narrowing due to intrinsic OPA bandwidth and saturation. Fig. 7 shows the measured spectra for stretched seed, amplified signal from the preamplifier and the power amplifier. In our configuration we saturate the OPCPA in order to obtain large extracted energy, at the expense of the recompressed pulse contrast level, which remains limited by the hard clip on the spectrum occurring in the pulse stretcher. Amplified signal spectrum is modulated by strong saturation in the power amplifier and resembles a top-hat shape. The measured output signal stability is greatly improved in the saturated regime, reducing the effect of pump energy variation and temporal jitter. We measured excellent beam quality (M^2=2) of the signal beam, as

expected in the process of optical parametric amplification, which conserves the signal beam quality to a very high degree.

We used a single-grating compressor to compress the signal pulse. The 1480 l/mm grating was set at 55.33 diffracted angle to match the stretcher angle. The compressor efficiency was 50%. We initially compressed the stretched seed pulses to 300 fs, limited by the spherical and chromatic aberrations occurring in the pulse stretcher containing a lens-based refractive telescope. Our calculations show negligible self-phase modulation (0.04 rad) due to short beam path through the gain medium, which is a significant advantage over regenerative multipass systems.

In summary, we demonstrated a successful use of optical parametric amplifiers for broadband, high fidelity chirped pulse amplification in place of regenerative amplifiers based on Ti:sapphire. In addition to possible applications as a stand-alone ultrafast pulse source, the wavelength and pulse energy level from our OPCPA is ideal for seeding high energy Nd:glass amplifiers of high power lasers. We expect the focused intensity from our system to be on the order of 10^{16} W/cm^2. Although our system did not exploit the full bandwidth capabilities of OPA, we demonstrated high gain, conversion efficiency and amplified pulse fidelity in OPCPA, which gives a viable cause for an all OPA-based kilojoule level ultrashort pulse source. With a suitable high energy pump laser and current compression grating technology, powers in excess of 10^{16} W are feasible using OPCPA.

5. Beam quality in optical parametric amplification

In this part of our study we focused on dephasing due to angular deviation from ideal phase matching in optical parametric amplification. Our model does not encompass any spatial, temporal and spectral effects, with a goal to isolate the effect of angular divergence on optical parametric amplification. Therefore, the calculations assume temporally continuous wave and monochromatic beams. Although the spatial frequency content of the beam is calculated from certain transverse beam profiles and used to evaluate its impact on OPA performance, this calculation evaluates only a "single" point on the beam intensity profile. This approach necessitates convolution with appropriate calculations for all values of intensity on the transverse beam profile and with walk-off calculations, but at the same time it provides insight into a particular aspect of optical parametric amplification which is frequently overlooked in calculations that take only spatial effects into account when predicting OPA performance. While in theory a possibility exists to ideally phase match plane waves, in actuality the beams will have finite transverse size. This will inevitably lead to non-vanishing angular deviation, even in perfect, transform limited beams. A detailed numerical evaluation of OPAs has to take this effect into account, particularly when beam quality of pump lasers is poor or the beam size is small, leading to large beam divergence.

In uniaxial crystals, phase matching is usually achieved along one propagation direction using beams of different polarizations. The extraordinary beam index of refraction is given by

$$n_e^2(\theta) = \frac{1}{\frac{\cos^2(\theta)}{n_o^2} + \frac{\sin^2(\theta)}{n_e^2}}, \tag{11}$$

where θ is the angle between the c-axis of the crystal and the beam, in the principal plane of the crystal, and n_o and n_e are indices of refraction for beams propagating in two orthogonal principal directions in the crystal. When the beam is not propagating along one of the crystal axes, the change of the index of refraction will be more sensitive to angular deviation in the principal plane of the crystal (critical phase matching). In

uniaxial crystals, detuning in the principal plane will be the dominant contribution to total angular detuning. Our general two-dimensional analysis for uniaxial crystals can therefore be reduced to a computationally less demanding one-dimensional case, where only detuning in the principal plane is considered. In biaxial crystals, critical phase matching is generally achieved in one of the principal planes of the crystal. In that case we can apply the same analysis to biaxial crystals, taking advantage of the large difference in angular sensitivity in the principal plane and perpendicular to the principal plane. A notable exception to this simplified treatment is the analysis of noncritically phase matched processes, where beam propagation is achieved along one of the principal axes. In that case, angular sensitivity has similar magnitude in both directions, requiring a full two-dimensional analysis.

In optical parametric devices, nonlinear crystals are commonly placed in the laser beam waist, which allows the laser intensity to rise to the level required for efficient parametric interactions and ensure best possible collimation. A perfect gaussian beam propagates according to the following equation:

$$w^2(z) = w_0^2\left(1+\left(\frac{\lambda(z-z_0)}{\pi w_0^2}\right)^2\right), \tag{12}$$

where by w we denote beam radius, w_0 beam waist radius, and z longitudinal position (z_0 being the waist position). In the beam waist, we can obtain one-dimensional distribution of electric field in spatial frequencies by taking the Fourier transform of the transverse electric field distribution:

$$E(s) = \int_{-\infty}^{\infty} E(x)e^{-isx}dx, \tag{13}$$

s denoting transverse spatial frequency. Fraunhoffer diffraction pattern in the far field is equivalent to the near-field distribution in spatial frequencies ($s=\theta/\lambda$). Therefore, any real laser beam will consist of a superposition of plane waves, with a distribution of divergence as indicated by the spatial frequency distribution. This divergence spread will contribute to dephasing in optical parametric amplification.

A formalism has been adopted for describing beam propagation when transverse beam quality differs from the ideal transform limit. Beam quality of a real beam can be described by the parameter M^2:

$$w^2(z) = w_0^2\left(1+\left(M^2\frac{\lambda(z-z_0)}{\pi w_0^2}\right)^2\right) \tag{14}$$

The meaning of the parameter M^2 is that a real beam will be diffracted in the far field with a divergence angle which is M^2 times greater than the divergence angle of a gaussian beam in TEM 00 mode. Equivalently, under same focusing conditions, the diameter of such beam in its waist will be M^2 times greater than the diameter of a beam with transform limited beam quality. Imperfect beam quality can be treated as an increase in the minimum beam waist – spatial frequency bandwidth product,

$$\sigma_{r0}\sigma_{s0} = \frac{M^2}{2\pi}, \tag{15}$$

where the beam waist σ_{r0} and spatial frequency bandwidth σ_{s0} are defined as variances of the beam intensity distribution in configuration and spatial frequency space, respectively, for radially symmetric beams. In our analysis we will consider two ideal beam profiles: gaussian, a common beam profile obtainable from laser resonators, and top-hat, favored for nonlinear conversion processes due to reduced spatial variation of gain and reduced Poynting vector walk-off effects. While most real beams used in optical parametric amplification will have beam profiles intermediate between the two ideal cases, this analysis still gives a quantitative assessment of expected conversion from real beams.

Perfect gaussian beam intensity distribution can be written in terms of intensity and amplitude:

$$I(r) = I_0\exp\left(-\frac{2r^2}{w^2}\right),\ E(r) = E_0\exp\left(-\frac{r^2}{w^2}\right). \tag{16}$$

The corresponding distribution in spatial frequencies is obtained by taking the Fourier transform of the electric field distribution $E(r)$:

$$E(s) = \pi E_0 w^2\exp\left(-\pi^2 s^2 w^2\right), \tag{17}$$

or, for beam that is not diffraction limited,

$$E(s)=\frac{\pi E_0 w^2}{M^4}\exp\left(-\frac{\pi^2 s^2 w^2}{M^4}\right). \tag{18}$$

Spatial frequency spectrum of the ideal top-hat beam can be calculated by taking the Hankel transform of the near-field electric field distribution:

$$E(s)=2\pi\int_0^\infty rE(r)J_0(2\pi rs)dr=2\pi E_0\int_0^w rJ_0(2\pi rs)dr=E_0w^2\frac{J_1(2sw)}{sw}, \tag{19}$$

where by J_0 and J_1 we denote zero and first order Bessel functions, respectively. For a beam with a beam quality parameter M^2, the spatial frequency spectrum will be

$$E(s)=\frac{E_0w^2}{M^4}\frac{J_1(2\pi sw/M^2)}{sw/M^2}. \tag{20}$$

Intensity distribution in spatial frequencies for a gaussian and a top-hat beam is

$$I(s)=2n\sqrt{\frac{\varepsilon_0}{\mu_0}}\left(\frac{\pi E_0w^2}{M^4}\right)^2\exp\left(-\frac{2\pi^2s^2w^2}{M^4}\right), \tag{21}$$

$$I(s)=2n\sqrt{\frac{\varepsilon_0}{\mu_0}}E_0^2\left(\frac{w}{M^2}\right)^4\left(\frac{J_1(2\pi sw/M^2)}{sw/M^2}\right)^2, \tag{22}$$

respectively.

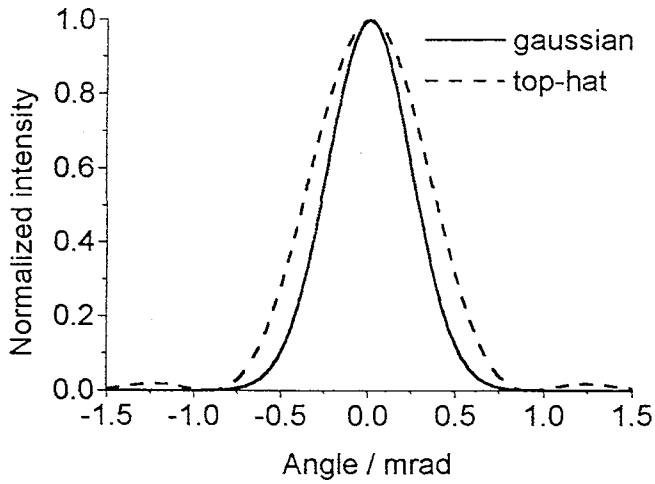

Figure 8.

In Fig. 8 we show normalized intensity distributions in divergence angles for gaussian TEM 00 and a top-hat radially symmetric beam of equal beam waist (radial intensity variance) σ_0=0.5 mm and λ=1064 nm. We note broader spatial frequency spectrum for a top-hat beam. While the spatial frequency variance cannot be evaluated for a top-hat beam with the accepted definition of beam quality, the calculated distribution for top-hat beam nevertheless allows quantitative analysis in OPAs. In addition, apodization in spatial frequency distribution is necessary for numerical evaluation, and is performed at $3w$ for gaussian beam, and at the secondary zero of the intensity distribution for Bessel beams. Apodization window has to be evaluated for every specific case in this type of analysis, ensuring that only negligible contribution to conversion is expected from the power distributed in spatial frequencies that are outside the apodization window.

In critical phase-matching, we reduce the general radial angular divergence intensity distribution to a one-dimensional distribution, with angular divergence in the crystal principal plane. We calculate the one-dimensional intensity distribution as

$$I_1(s_x) = C\int_{-\infty}^{\infty} I\left(\sqrt{s_x^2 + s_y^2}\right) ds_y , \tag{23}$$

where by s_x and s_y we label spatial frequencies in two principal directions, $I_1(s_x)$ one-dimensional intensity distribution and $I(r)$ radial intensity distribution in spatial frequencies. C is the normalization constant, such that

$$\int_{-\infty}^{\infty} I_1(s_x)\, ds_x = \int_0^{\infty} I(s) 2\pi s ds . \tag{24}$$

We can calculate the spread in spatial frequencies if we know the beam quality parameter and focusing conditions. In practice, for measured beam quality, we can determine beam size that will exhibit acceptable amount of dephasing. Another consideration present in OPAs is the depth of focus, which will lead to nonuniform beam intensity along the amplifier. In the present discussion we will neglect variable intensity effects as we are mostly interested in nanosecond OPAs, with relatively weak focusing and long depth of focus compared to the OPA length. Also, Guoy phase shift that occurs on relatively short scale when tightly focused beams are used will not be relevant to our calculation with weakly focused beams and short crystals.

We represent the total electric field as a superposition of plane waves with angular distribution identical to the one-dimensional electric field distribution in angles:

$$\mathbf{E}_j = \sum_i A_{ji}\mathbf{e}_{ji}\exp[-i(\omega_j t - \mathbf{k}_{ji}\mathbf{r})], \quad j = 1,2,3 \tag{25}$$

where e_{ji} represents the unit vector in the propagation direction of the corresponding plane wave, and A_{ji} represents the amplitude of an individual plane wave, normalized to the intensity of the corresponding beam:

$$\sum_i A_{ji}^2 = \frac{\mu_0}{\varepsilon_0}\frac{I_j}{2n_j}, \quad j = 1,2,3. \tag{26}$$

We note that an approximation can be made: $k_{ji}r=k_{ji}z$, as a consequence of paraxial beam propagation. Now we can solve coupled differential equations that govern difference frequency generation:

$$\begin{aligned}
\frac{dA_{1k(i,j)}}{dz} &= i\frac{2\omega_1 d_{eff}}{n_1 c}\sum_i\sum_j A_{2i}^* A_{3j}\exp\left(i\Delta k_{ijk} z\right),\\
\frac{dA_{2k(i,j)}}{dz} &= i\frac{2\omega_2 d_{eff}}{n_2 c}\sum_i\sum_j A_{1i} A_{3j}^*\exp\left(i\Delta k_{ijk} z\right),\\
\frac{dA_{3k(i,j)}}{dz} &= i\frac{2\omega_3 d_{eff}}{n_3 c}\sum_i\sum_j A_{2i} A_{3j}\exp\left(-i\Delta k_{ijk} z\right),
\end{aligned} \tag{27}$$

where by *k(i,j)* we denote the mapping function, which assigns the appropriate component of the third wave resulting from the interaction between the components *i* and *j* of the remaining two waves. The mapping function is a direct result of the nonlinear Snell's law, which defines he propagation angles for three waves interacting in a nonlinear medium. We can now assign a unique wavevector mismatch to all combinations of plane wave components that interact at a particular position in crystal, which makes this analysis distinct from a simple treatment that approximates the beam with a single plane wave with weight-averaged angular deviation.

We solve the system of coupled differential equations by the 4th order Runge-Kutta method for numerical integration. The required number of the integration steps and the tranverse mesh size are determined by testing the result convergence with increasing grid finesse. Our typical calculations were carried out with 50 points in the spatial frequency domain and 1000 step in numerical integration per 1 cm crystal length. Our

analysis tracks the electric field amplitude and phase throughout the interaction region, after which we calculate total beam intensity and gain.

In order to quantify the average divergence in our calculations, we introduce the pump beam divergence parameter α:

$$\alpha = \frac{M^2 \lambda}{w}. \tag{28}$$

Divergence parameter takes into account beam size, wavelength and beam quality, resembling the far-field diffracted angle. We now proceed to calculate the influence of beam quality on small signal gain in OPA. The simulation parameters are: I_p=500 MW/cm^2, I_{seed}=10^{-3} W/cm^2, λ_p=532 nm, λ_s=1054 nm. The difference frequency mixing process is 1054 nm (o) + 1074 nm (o) = 532 nm (e). Minimum beam size – spatial frequency bandwidth product is assumed for the incident seed beam, corresponding to experimentally relevant case of amplification of a high quality seed beam using an energetic pump beam of less than ideal beam quality.

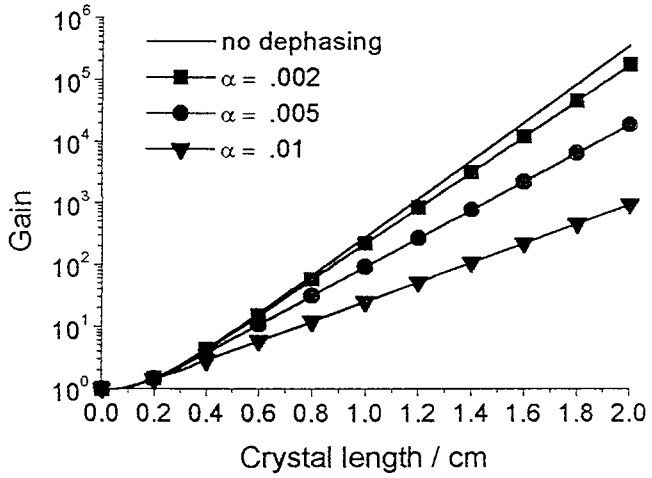

Figure 9.

Fig. 9 shows small signal gain in BBO as a function of interaction length in crystal, for several divergence parameters α and gaussian beams. Indicated in Fig. 9 is the result of our model calculation when no dephasing (Δk=0) is assumed, and it is in agreement with a simple calculation based on a single, perfectly phase matched plane

wave. Identical calculation is performed with a top-hat beam, with results shown in Fig. 10. It is apparent that reduction of gain will occur even for modest values of divergence parameter α, consistent with relatively narrow angular acceptance of BBO. We also observe that the gain reduction is more severe for a top-hat beam than for a gaussian beam with the same divergence parameter α, resulting from broader angular intensity distribution for a top-hat beam compared to a gaussian beam with the same beam waist w.

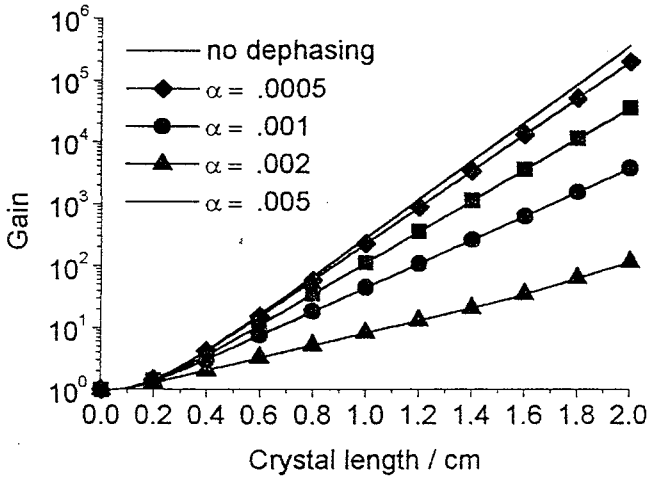

Figure 10.

To evaluate maximum conversion efficiency in OPA we need to analyze large signal gain configurations. Our analysis proceeds to calculate gain in configuration when $P_{pump}= 5P_{seed}$, leading to strong depletion of the pump wave and back-conversion. Results for BBO are shown again in Figs. 11-12, for gaussian and top-hat beam profiles. It is important to note an important difference between our results and the results of simple calculations in which single plane wave with a single averaged value of phase mismatch is considered. While calculations with single plane wave result in cycles of conversion and back-conversion which occur with specific frequency and consistently attain same maxima and minima, our results show conversion behavior similar to the behavior of a damped oscillator, where successive oscillations become less pronounced. This is the result of a large number of plane waves interacting with variable phase mismatch and subsequent different conversion and back-conversion rates for plane wave components across the spatial frequency spectrum.

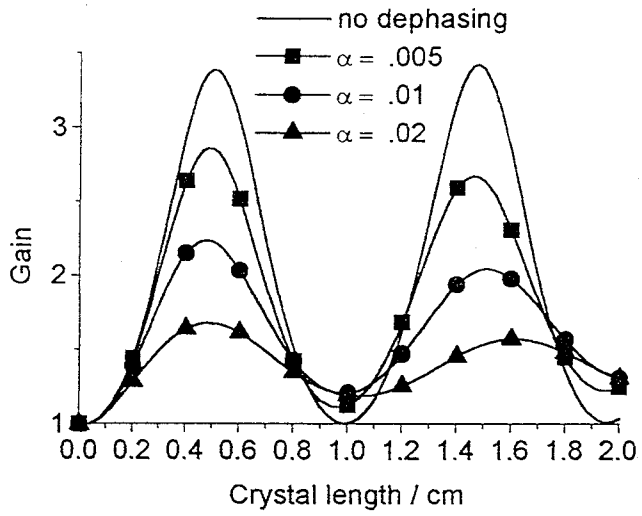

Figure 11.

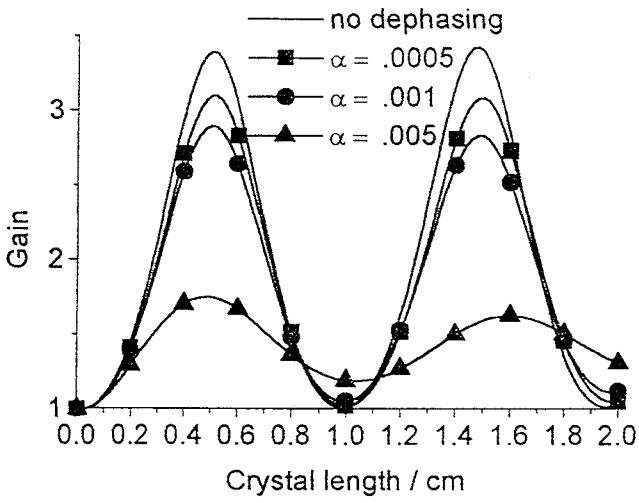

Figure 12.

The analysis of OPA performance for gaussian and top-hat beams leads to an observation that while top-hat beams are known to produce most efficient conversion in optical parametric amplification due to their superior spatial performance, there is an important property of gaussian beam interaction which makes gaussian beams less sensitive to angular divergence in optical parametric amplification. When we compare the spatial frequency spectrum of gaussian and top-hat beams, we find that a gaussian beam has a relatively sharp drop-off and large energy content concentrated in its only, central lobe of the spatial frequency spectrum. If we make a comparison between a gaussian and

a top-hat beam of same beam size and consider the cut-off point in the spatial frequency spectrum at the first zero of the Bessel function for top-hat beam, then the top-hat beam has only 84%, while the gaussian has 99.9% of its energy concentrated in the same enclosed area. We argue that this difference is responsible for observed variation in angular sensitivity for gaussian and top-hat beams. Common nonlinear crystals in critically phase-matched configurations typically exhibit narrow angular tolerances, frequently allowing only the central lobe of the spatial frequency spectrum of a top-hat beam inside their angular bandwidth for optical parametric amplification. Coupled with strongly nonlinear dependence of difference frequency generation on the beam intensity, a significant drop in gain is expected with reduced effective beam intensity. The conclusion drawn from this picture is fully consistent with the calculated difference in behavior between gaussian and top-hat beams in optical parametric amplification in the small signal regime. This difference is visible when we evaluate gain in the strongly depleted regime as well, arising from the fact that the pump angular components in large spatial frequencies will experience rapid cycles of conversion and back-conversion, not contributing significantly to the overall conversion.

Eimerl[16] has previously studied second harmonic generation and concluded that the conversion efficiency in second harmonic generation is determined exclusively by the beam peak power and beam quality in critically phase matched crystals. While increasing the beam intensity by telescoping the beam may decrease the required crystal length, there is no impact on overall conversion efficiency. This result can be extended to optical parametric amplification, and can be seen best from simplified expression for small signal gain

$$G = \frac{1}{4}\exp(2g_0 L)\operatorname{sinc}^2\left(\frac{\Delta kL}{2}\right), \tag{29}$$

$$g_0 = 4\pi d_{eff}\sqrt{\frac{I_p}{2\varepsilon_0 n_p n_s n_i c\lambda_s \lambda_p}} = K\sqrt{I_p}, \tag{30}$$

where I_p is the intensity of the pump. In critical phase matching, wavevector mismatch Δk can be approximated by linear function of divergence angle for small angles:

$$\Delta kL = \beta_\theta \Delta\theta L = \frac{\beta_\theta}{4}\frac{M^2\lambda}{\pi w}L, \tag{31}$$

where β_θ is the angular sensitivity for a critically phase-matched nonlinear crystal ($\beta_\theta = d(\Delta k)/d\theta$). We can now rewrite the expression for small signal gain for rotationally symmetric beams as

$$G = \frac{1}{4}\exp\left(\frac{2K}{\sqrt{\pi}}\sqrt{P_p}\frac{L}{w}\right)\mathrm{sinc}^2\left(\frac{\beta_\theta}{8}\frac{M^2\lambda}{\pi}\frac{L}{w}\right), \tag{32}$$

where P_p denotes the peak power of the pump beam. We notice that while telescoping the beam changes beam size w, the ratio L/w remains invariant for same gain. The problem of obtaining maximum gain, therefore, reduces to selecting proper ratio of crystal length and beam size for particular pump peak power.

Dephasing can be reduced in uniaxial crystals by using elliptical beams, elongated in the principal plane of the crystal. Elliptical beams take advantage of the anisotropy in angular sensitivity, reducing dephasing while enabling the same pump intensity. Dephasing is reduced by a factor of $\sqrt{A}$, where A is the beam aspect ratio, compared to a radially symmetric beam of the same intensity. As a consequence, beam quality parameter M^2 can be $\sqrt{A}$ times larger compared to a radially symmetric beam. The limit of usability of this scheme in uniaxial crystals is determined by dephasing due to divergence in the insensitive direction, which starts to compete with dephasing due to divergence in the sensitive direction at certain large aspect ratio. We calculate this aspect ratio in BBO to be ~20.

Another advantage of using elliptical beams in uniaxial crystals is the reduction of walk-off effects. Walk-off occurs for extraordinary polarized beam and is directed in the crystal sensitive direction, with a characteristic angle ρ. Then improved overlap of ordinary and extraordinary elliptical beams will result in better conversion efficiency. This effect can severely impact conversion efficiency, particularly when intersecting beams are small and interaction lengths are long.

In noncritical phase-matching, phase mismatch can be approximated by a quadratic dependence on the divergence angle

$$\Delta kL = \gamma_\theta \Delta\theta^2 L = \frac{\gamma_\theta}{16}\left(\frac{M^2\lambda}{\pi w}\right)^2 L = \frac{\gamma_\theta}{16}\frac{M^4\lambda^2}{\pi^2 w}\frac{L}{w}, \tag{33}$$

where by γ_θ we denote angular sensitivity $d^2(\Delta k)/d\theta^2$. Conversion efficiency can be increased in noncritically phase matched crystals by increasing the beam size. Contrary to intuition, weaker beam focusing enables higher conversion in noncritically phase matched crystals. The obvious limit of practicality of this result is the availability of large crystals of sufficient quality, and the contributions to dephasing that are directly proportional to crystal length, such as spectral bandwidth.

In a simplified analysis, we now derive the criterion for beam quality that allows high conversion efficiency to be extracted in optical parametric amplifiers. In Eq. (32) we have seen that if we neglect dephasing, small signal gain can be obtained for certain value of peak power available by selecting the appropriate ratio of crystal length and beam size

$$L/w = \frac{\sqrt{\pi}}{2K\sqrt{P}}\ln(4G), \tag{34}$$

Dephasing term for the selected ratio *L/w* will be

$$\operatorname{sinc}^2\left(\frac{\Delta kL}{2}\right) = \operatorname{sinc}^2\left(\frac{\beta_\theta}{2}\times\frac{1}{2}\frac{M^2\lambda}{2\pi w}L\right) = \operatorname{sinc}^2\left(\frac{\beta_\theta}{16\sqrt{\pi}}\frac{M^2\lambda\ln(4G)}{K\sqrt{P}}\right), \tag{35}$$

$$\operatorname{sinc}^2\left(\frac{\Delta kL}{2}\right) = \operatorname{sinc}^2\left(\frac{\gamma_\theta}{2}\times\frac{1}{2}\left(\frac{M^2\lambda}{2\pi w}\right)^2 L\right) = \operatorname{sinc}^2\left(\frac{\gamma_\theta}{32\pi^{3/2}}\frac{M^4\lambda^2\ln(4G)}{Kw\sqrt{P}}\right), \tag{36}$$

for critically and noncritically phase matched crystals, respectively. If we define demand for high conversion efficiency with $\operatorname{sinc}^2(\Delta kL/2) > 0.5$, or $\Delta kL/2 < 1.39$, we now have a criterion for required beam quality for lasers pumping OPAs:

$$M^2 < 1.39\times 16\sqrt{\pi}\frac{K\sqrt{P}}{\beta_\theta\lambda\ln(4G)}, \tag{37}$$

$$M^2 < 1.39\times 32\pi^{3/2}\frac{Kw\sqrt{P}}{\gamma_\theta\lambda^2\ln(4G)}, \tag{38}$$

for critically and noncritically phase matched crystals, respectively. For a particular nonlinear crystal, beam quality required to produce efficient conversion in critically phase matched crystals will be dependent on crystal properties, peak power available from laser, desired gain and wavelengths of three interacting waves. In addition to these parameters, beam quality requirements in noncritically phase matched crystals depend also on the beam size, being less stringent for larger beams.

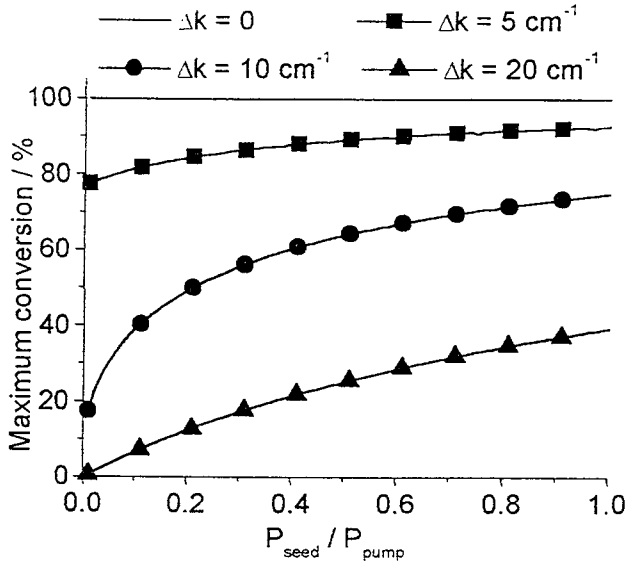

Figure 13.

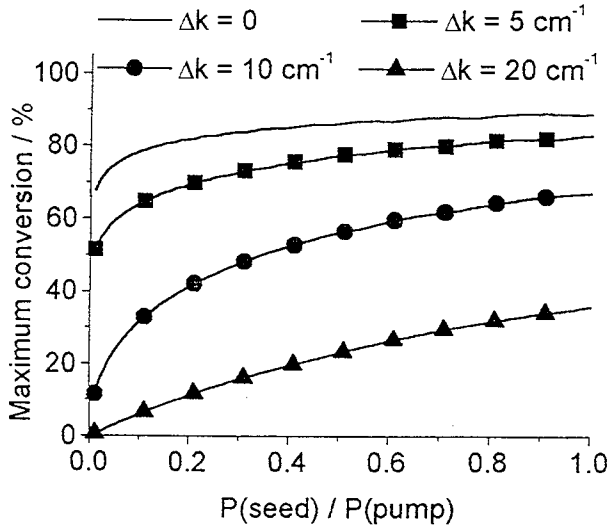

Figure 14.

An important consideration in OPA design concerns a simple difference between harmonic generation and seeded OPAs. While second harmonic generators build up without an incident harmonic beam, seeded OPAs have radically different boundary conditions, where seed beam intensity is typically many orders of magnitude greater than the zero-point field fluctuation. Seed power will, therefore, influence the overall conversion efficiency in OPA. We performed a simple calculation to determine

maximum conversion in OPA as a function of seed power. Our results are shown in Fig. 13, without walk-off, and in Fig. 14, with included walk-off effect. Shown is the maximum conversion of the pump beam to signal and idler as a function of the ratio of seed and pump peak power, for different values of wavevector mismatch Δk. A single plane wave with wavevector mismatch Δk is assumed. The evaluated mixing process is 1054 nm (o) + 1074 nm (o) = 532 nm (e), with pump waist size 2 mm (top-hat), and pump intensity of 1 GW/cm^2. Maximum conversion is found by varying the crystal size with constant input intensity. With Δk=0 and in absence of walk-off, maximum conversion is 100% and it is independent of the seed power. As wavevector mismatch increases, we note that higher conversion efficiency is possible when the input seed intensity increases. When we include walk-off, even zero wavevector mismatch leads to maximum conversion of ~85% when P_{seed}/P_{pump}=1. Even in this case we can improve efficiency by increasing the ratio P_{seed}/P_{pump}, asymptotically approaching 100% conversion when $P_{seed}/P_{pump}\rightarrow\infty$.

As a result of optical parametric amplification, the idler wave is generated at the difference frequency between the pump wave and the signal wave. A difference between the signal and the idler wave is that the signal wave retains its angular content, while the angular spectrum of the idler wave is broader. The reason for this is that in seeded OPAs, signal builds up from a field which is orders of magnitude higher in intensity than the spontaneous emission. This asymmetry is then preferentially projected to the idler wave, which acquires angular components resulting from interaction of pump and signal waves, both with specific angular content. Idler beam will exhibit worse beam quality than signal and pump beam, and while its applicability may remain satisfactory, optical parametric amplification can be regarded as a process in which signal beam is amplified with high fidelity, while phase and angular aberrations transferred to the idler beam. In addition to the angular aberrations, other sources of dephasing in optical parametric amplification will contribute to the idler phase content.

Our model, based on plane wave decomposition, can be used to isolate and evaluate the influence of spatial frequency content of real laser beams on performance of devices based on optical parametric amplification. Our evaluation of beams with gaussian and top-hat spatial intensity profile resulted in the conclusion that top-hat beams exhibit

greater sensitivity to angular dephasing than gaussian beams, arising from broadly distributed angular spectrum of the top-hat beam. This important consideration should be incorporated into analysis and prediction of performance for parametric devices, frequently using top-hat beams due to their reduced walk-off and transversely variable conversion problems. Additionally, calculated idler angular and phase content is consistent with the view of optical parametric amplification as process which conserves seed beam fidelity, channeling the phase and angular aberrations into idler wave.

We determined that conversion efficiency in optical parametric amplification depends on seed and pump peak power, beam spatial frequency content and nonlinear medium properties. While beam resizing has no impact on conversion efficiency in critically phase matched devices, increasing the beam size is favored for noncritically phase matched devices. Beam quality requirements can be relaxed by using elliptical beams in critically phase matched crystals. We also determined practical requirements on beam quality for gaussian and top-hat beams.

We expect that our model and code will be useful in making corrections to existing codes that treat difference frequency generation only in spatial and temporal domain, while averaging the effects in the spatial frequency space. Although incorporation of this code into a larger, comprehensive code for optical parametric amplification will require significantly greater computational power, its value still remains in providing insight into angular effects in optical parametric amplifiers and estimating their relative magnitude.